



HAL
open science

The response of pre-osteoblasts and osteoclasts to gallium containing mesoporous bioactive glasses

N. Gómez-Cerezo, E. Verron, V. Montouillout, F. Fayon, P. Lagadec, J. -M. Bouler, B. Bujoli, D. Arcos, M. Vallet-Regí

► To cite this version:

N. Gómez-Cerezo, E. Verron, V. Montouillout, F. Fayon, P. Lagadec, et al.. The response of pre-osteoblasts and osteoclasts to gallium containing mesoporous bioactive glasses. *Acta Biomaterialia*, 2018, 76, pp.333 - 343. 10.1016/j.actbio.2018.06.036 . hal-01898580

HAL Id: hal-01898580

<https://hal.science/hal-01898580>

Submitted on 11 Apr 2022

HAL is a multi-disciplinary open access archive for the deposit and dissemination of scientific research documents, whether they are published or not. The documents may come from teaching and research institutions in France or abroad, or from public or private research centers.

L'archive ouverte pluridisciplinaire **HAL**, est destinée au dépôt et à la diffusion de documents scientifiques de niveau recherche, publiés ou non, émanant des établissements d'enseignement et de recherche français ou étrangers, des laboratoires publics ou privés.



Full length article

The response of pre-osteoblasts and osteoclasts to gallium containing mesoporous bioactive glasses



N. Gómez-Cerezo^{a,b}, E. Verron^c, V. Montouillout^d, F. Fayon^d, P. Lagadec^e, J.M. Bouler^c, B. Bujoli^c, D. Arcos^{a,b,*}, M. Vallet-Regí^{a,b,*}

^a Departamento de Química en Ciencias Farmacéuticas, Facultad de Farmacia, Universidad Complutense de Madrid, Instituto de Investigación Sanitaria Hospital 12 de Octubre i+12, Plaza Ramón y Cajal s/n, 28040 Madrid, Spain

^b CIBER de Bioingeniería Biomateriales y Nanomedicina (CIBER-BBN), Spain

^c Université de Nantes, CNRS, UMR 6230, CEISAM, UFR Sciences et Techniques, 2 Rue de la Houssinière, 44322 NANTES Cedex 3, France

^d CNRS, UPR 3079, CEMHTI, 1D Avenue de la Recherche Scientifique, 45071 Orléans Cedex 02, France

^e Université Côte d'Azur, CNRS, Inserm, Institut de Biologie Valrose (iBV), 28 Av. de Valombrose, 06107 Nice Cedex 2, France

ARTICLE INFO

Article history:

Received 23 March 2018

Received in revised form 11 June 2018

Accepted 28 June 2018

Available online 30 June 2018

Keywords:

Gallium

Mesoporous bioactive glasses

Osteoblast

Osteoclast

Osteoporosis

ABSTRACT

Mesoporous bioactive glasses (MBGs) in the system $\text{SiO}_2\text{-CaO-P}_2\text{O}_5\text{-Ga}_2\text{O}_3$ have been synthesized by the evaporation induced self-assembly method and subsequent impregnation with Ga cations. Two different compositions have been prepared and the local environment of Ga(III) has been characterized using ^{29}Si , ^{71}Ga and ^{31}P NMR analysis, demonstrating that Ga(III) is efficiently incorporated as both, network former (GaO_4 units) and network modifier (GaO_6 units). *In vitro* bioactivity tests evidenced that Ga-containing MBGs retain their capability for nucleation and growth of an apatite-like layer in contact with a simulated body fluid with ion concentrations nearly equal to those of human blood plasma. Finally, *in vitro* cell culture tests evidenced that Ga incorporation results in a selective effect on osteoblasts and osteoclasts. Indeed, the presence of this element enhances the early differentiation towards osteoblast phenotype while disturbing osteoclastogenesis. Considering these results, Ga-doped MBGs might be proposed as bone substitutes, especially in osteoporosis scenarios.

Statement of Significance

Osteoporosis is the most prevalent bone disease affecting millions of patients every year. However, there is a lack of bone grafts specifically designed for the treatment of bone defects occurred because of osteoporotic fractures. The consequence is that osteoporotic bone defects are commonly treated with the same biomaterials intended for high quality bone tissue. In this work we have prepared mesoporous bioactive glasses doped with gallium, demonstrating osteoinductive capability by promoting the differentiation of pre-osteoblast toward osteoblasts and partial inhibition of osteoclastogenesis. Through a deep study of the local environment of gallium within the mesoporous matrix, this work shows that gallium release is not required to produce this effect on osteoblasts and osteoclasts. In this sense, the presence of this element at the surface of the mesoporous bioactive glasses would be enough to locally promote bone formation while reducing bone resorption.

© 2018 Acta Materialia Inc. Published by Elsevier Ltd. All rights reserved.

1. Introduction

Mesoporous bioactive glasses (MBGs) are a kind of bioceramics with potential application for bone tissue regeneration purposes.

Since Yan et al prepared MBGs for the first time in 2004 [1], these materials have arisen great interest in the field of regenerative medicine of bone due to their excellent bioactive properties, which have been demonstrated both *in vitro* [2,3] and *in vivo* [4,5]. MBGs are commonly synthesized in the ternary $\text{SiO}_2\text{-CaO-P}_2\text{O}_5$ system, with similar chemical compositions to those used for conventional bioactive sol-gel glasses [2,6,7]. However, the incorporation of a structure directing agent during the hydrolysis and condensation processes leads to the formation of a mesophase, which eventually results into ordered

* Corresponding authors at: Departamento de Química en Ciencias Farmacéuticas, Facultad de Farmacia, Universidad Complutense de Madrid, Instituto de Investigación Sanitaria Hospital 12 de Octubre i+12, Plaza Ramón y Cajal s/n, 28040 Madrid, Spain.

E-mail addresses: arcosd@ucm.es (D. Arcos), vallet@ucm.es (M. Vallet-Regí).

mesoporous structures with very high surface areas and porosities [8]. The bone regeneration properties of bioglasses come up from their capability to exchange ions with the surrounding fluids, mainly Ca^{2+} by H^+ , with the subsequent growth of an apatite-like phase on the surface, similar to the mineral component of bones and teeth [9]. Besides, the dissolution products of bioactive glasses (Ca^{2+} and silica species in solution) elicit the upregulation of pro-osteoblastic genes [10–12] thus enhancing their osteogenic potential.

The high surface area and porosity of MBGs accelerate the chemical reactions at the implants surface and, consequently, MBGs exhibit the fastest bioactive behaviour observed so far in the field of bioceramics [13]. The ordered mesoporous structure of MBGs brings about their potential applications as drug delivery systems [14] and are excellent matrixes to host and release active agents such as antibiotics [15], antiosteoporotics [16] or antitumoral drugs [17], which can even be released in a stimulatory manner [18,19].

The efficiency of MBGs to trigger the ionic exchange with the surrounding fluids has recently fostered their application as carriers of therapeutic ions. In this way species, such as Li^+ , Sr^{2+} , Cu^{2+} , Co^{2+} or B^{3+} have been incorporated into $\text{SiO}_2\text{-CaO-P}_2\text{O}_5$ MBGs, with the aim of providing osteogenic, cementogenic, angiogenic and antibacterial properties [20,21–24]. The release of these chemical species can yield very interesting synergies with the bioactive behaviour of MBGs and the pharmacological treatment loaded in the mesopores. Therapeutic ions are commonly incorporated to MBGs as inorganic salts dissolved together with the MBGs precursors. At the end of the synthesis these ions can stay in the MBGs associated to phosphates or as network modifiers of the silica matrix, similarly to the role played by calcium cations [25–29]. In most cases, the large volume and/or the polarization capacity of these ions are so intense that even low concentrations lead to the disorganization of the mesoporous structure [30].

One of the most interesting therapeutic ions in the field of bone pathologies is Ga (III). The inhibition of bone resorption driven by Ga (III) has been widely reported [31–35]. Ga reduces the resorption activity, differentiation and formation of osteoclasts without cytotoxic effects in a dose-dependent manner, pointing out an excellent potential for the treatment of osteoporotic bone fractures associated to bone implants [36,37]. In this sense, Ga ions have been successfully combined with apatitic calcium phosphate cements and tested both *in vitro* and *in vivo* [38].

Although some studies have been carried out describing the effects of Ga^{3+} on the structure of MBGs [39–42], as well as haemostatic and antibacterial effects [43], from the best of our knowledge no study has considered the effects of Ga containing MBGs on bone cells, such as osteoblasts or osteoclasts. This is quite surprising considering the very interesting synergy between Ga^{3+} and MBGs for the treatment of osteoporotic bone fractures. Moreover, contrarily to monovalent or divalent Cu(II) , Co(II) , Sr(II) , Li(I) , etc. cations, which act as modifiers of the silica network when incorporated into MBGs, Ga (III) cations can act as both network formers (NF) and network modifier (NM). The distribution and local environment of Ga species into MBGs are still poorly understood and the influence of Ga on bone remodelling cannot be explained without understanding the relationship between the local structure of this inhibitor of bone resorption with the resulting biological response.

In this paper we evaluate for the first time the biological response of Ga doped MBGs with respect to bone forming cells (osteoblasts) and bone resorptive cells (osteoclasts), together with a deep study of the local environment of this cation into the mesoporous matrix of these bioceramics.

2. Materials and methods

2.1. Synthesis of materials

Two different MBGs in the system $\text{SiO}_2\text{-CaO-P}_2\text{O}_5$ were synthesized by evaporation induced self-assembly (EISA) method [44]. For this aim, triblock copolymer F127 $(\text{EO})_{100}\text{-(PO)}_{65}\text{-(EO)}$ was used as structure directing agent. Tetraethyl orthosilicate (TEOS) (98%), triethyl phosphate (TEP) (99%) and calcium nitrate tetrahydrate $\text{Ca}(\text{NO}_3)_2\cdot 4\text{H}_2\text{O}$ (99%) were used as SiO_2 , P_2O_5 and CaO sources, respectively. In a typical synthesis 2 g of surfactant were dissolved in ethanol with HCl 0.5 M solution at room temperature. Afterward TEOS, TEP and $\text{Ca}(\text{NO}_3)_2\cdot 4\text{H}_2\text{O}$ were added under stirring in 3 h intervals to obtain two different MBG denoted MBG-58S and MBG-85S. The different reagents and amounts are shown in Table 1. The resulting solution was kept under stirring for 12 h and poured into Petri dishes (9 cm in diameter). The colourless solution was evaporated at 30 °C for 7 days. Eventually, the dried gels were removed as homogeneous and transparent membranes and calcined at 700 °C for 3 h under air atmosphere.

Solids MBG-58SGa and MBG-85SGa were synthesized from MBG-58S and MBG-85S respectively. In a typical procedure, a certain amount of $\text{Ga}(\text{NO}_3)_3\cdot 4\text{H}_2\text{O}$ was dissolved in a vessel containing 100 mL of ultrapure water. Then 500 mg of the corresponding MBG (MBG-58S or MBG-85S) were added to the solution in such a way that the Ga/Ca molar ratio was 0.38 (see Table 1). The pH of the solution was adjusted in the 9.2–9.8 range by means of a concentrated ammonia solution. The mixture was stirred for 24 h at room temperature and the solids obtained were filtered under vacuum. Finally, solids were dried at 100 °C for 24 h. All reactants were purchased from Aldrich and used without further purification.

2.2. Physicochemical characterization of MBGs

Low angle powder X-ray diffraction experiments were performed with a Philips X'Pert diffractometer equipped with $\text{Cu K}\alpha$ radiation (wavelength 1.5406 Å). XRD patterns were collected in the 2 θ° range between 0.5 and 6.5 with a step size of 0.02 2 θ° and counting time of 4 s per step.

The textural properties of the calcined materials were determined by nitrogen adsorption with a Micromeritics ASAP 2010 equipment. To perform the N_2 adsorption measurements, the samples were previously degassed under vacuum for 20 h, at 100 °C. The surface area was determined using the Brunauer-Emmett-Teller (BET) method. The pore size distribution between 0.5 and 40 nm was determined from the adsorption branch of the isotherm by means of the Barret-Joyner-Halenda (BJH) method. This experiment was made in triplicate using different batches of each sample.

Chemical compositions of MBGs were determined by X-ray fluorescence (XRF) spectroscopy, using a Philips PANalytical AXIOS spectrometer (Philips Electronics NV), with X-rays generated by the $\text{RhK}\alpha$ line at $\lambda = 0.614$ Å.

^{29}Si MAS and $\{^1\text{H}\}\text{-}^{29}\text{Si}$ CP-MAS NMR spectra were recorded on a Bruker Avance 400WB spectrometer operating at a magnetic field

Table 1
Amounts of reagents used for the synthesis of the MBGs.

Sample	TEOS (g)	TEP (g)	$\text{Ca}(\text{NO}_3)_2\cdot 6\text{H}_2\text{O}$ (g)	$\text{Ga}(\text{NO}_3)_3\cdot 4\text{H}_2\text{O}$ (g)
MBG-58S	3.49	0.51	2.47	–
MBG-58SGa	3.49	0.51	2.47	0.1
MBG-85S	3.70	0.34	0.49	–
MBG-85SGa	3.70	0.34	0.49	0.026

of 9.4 T (^{29}Si Larmor frequency of 79.5 MHz) at a spinning frequency of 12 kHz. The ^{29}Si quantitative MAS spectra were acquired using a 90° flip angle with a recycling delay of 5 s and around 10,000 scans were co-added. The $\{^1\text{H}\}$ - ^{29}Si CP-MAS spectra were recorded using a contact time of 3.5 ms. 135,000 transients were co-added with a recycle delay of 5 s. The ^{71}Ga NMR experiments were performed on a Bruker Avance III spectrometer operating at 20.0 T (^{71}Ga Larmor frequency of 259.3 MHz) equipped with a 1.3 mm double-resonance MAS probe head. The ^{71}Ga central transition (CT)-selective MAS spectra were recorded using a Hahn echo sequence with whole echo acquisition. The echo delay was synchronized with the rotor period and the rf-field strength was 60 kHz corresponding to a CT-selective $\pi/2$ pulse of 2.1 μs . Approximately, 28 000 transients were accumulated for MBG-58SGa and 122 500 for MBG-85SGa with 0.5 s recycling delay. The ^{31}P quantitative MAS spectra were recorded using single pulse ($\pi/10$) acquisition; ~ 500 scans were co-added with a recycle delay of 120 s to ensure complete recovering of the longitudinal magnetization. ^1H SPINAL-64 decoupling with a nutation frequency of 70 kHz was applied during signal acquisition [45]. Chemical shift values were referenced to tetramethylsilane (TMS), H_3PO_4 and $\text{Ga}(\text{NO}_3)_3 \cdot 4\text{H}_2\text{O}$ for ^{29}Si , ^{31}P and ^{71}Ga , respectively.

Transmission electron microscopy (TEM) was carried out using a JEOL-2100 microscope, operating at 300 kV (Cs 0.6 mm, resolution 1.7 Å). Images were recorded using a CCD camera (model Keen view, SIS analyses size 1024×1024 , pixel size $23.5 \text{ mm} \times 23.5 \text{ mm}$) at $30000\times$ and $60000\times$ magnification using a low-dose condition.

2.3. *In vitro* bioactivity tests

Assessments of *in vitro* bioactivity were carried out on powder samples. For this purpose, 50 mg of powder were soaked into 7 mL of filtered simulated body fluid (SBF), in polyethylene containers at 37°C under sterile conditions. SBF solution was prepared according to Kokubo et al. [46] by dissolving NaCl, KCl, NaHCO_3 , $\text{K}_2\text{HPO}_4 \cdot 3\text{H}_2\text{O}$, $\text{MgCl}_2 \cdot 6\text{H}_2\text{O}$, CaCl_2 , and Na_2SO_4 into distilled water. It was buffered at $\text{pH} = 7.38$ by using tris(hydroxymethyl)-amino methane/HCl (TRIS/HCl) and then passed through 0.22 μm Millipore filters to avoid bacterial contamination. To avoid false positive responses, we included $\alpha\text{-Al}_2\text{O}_3$ as inert control (Fig S5 in Supporting Information). The evolution of the glass surface was analysed by Fourier transform infrared (FTIR) spectroscopy with a Nicolet Magma IR 550 spectrometer and by scanning electron microscopy (SEM) using a JEOL F-6335 microscope. To assess the Ca^{2+} - H^+ ionic exchange between MBGs and SBF, calcium concentration and pH changes were analysed as a function of soaking time by using an Ilyte $\text{Na}^+ \text{K}^+ \text{Ca}^{2+}$ pH system. All the experiments were carried out in triplicate.

2.4. Ga *In vitro* release

Ga release study was performed suspending 2 mg of solids in 2 mL of α -MEM (Sigma Chemical Company, St. Louis, MO, USA). 0.5 mL of this suspension was placed on a transwell permeable support with polycarbonate membrane (0.4 μm). The well was filled with 1.5 mL of α MEM and the suspension was stirred at 37°C at 100 rpm for 10 days. The amount of Ga released was determined by inductively coupled plasma spectroscopy (ICP), and the solution outside the transwell insert was replaced with fresh medium after each measurement. All the experiments were carried out in triplicate.

2.5. Pre-osteoblast cell culture tests

Murine MC3T3-E1 pre-osteoblasts ($2 \cdot 10^4$ cell/mL) were cultured in α -MEM with 10% fetal bovine serum (FBS, Gibco,

BRL), 1 mM L-glutamine (BioWhittaker Europe, Belgium), penicillin ($200 \text{ mg} \cdot \text{mL}^{-1}$, BioWhittaker Europe, Belgium), and streptomycin ($200 \text{ mg} \cdot \text{mL}^{-1}$, BioWhittaker Europe, Belgium), under a CO_2 (5%) atmosphere at 37°C for 12 h to reach the confluence in each cell plate. After that the MBGs powders were added on the cells at 1 mg/ml of concentration.

2.5.1. Fluorescence microscopy assays

To evaluate cells morphology after 4 days in contact with the materials, MC3T3-E1 cells were cultured in 24 well plates at density of 10^4 cells/mL in the presence of 1 mg/mL of the different MBGs. Thereafter, cells were rinsed with PBS twice and fixed in 4% (w/v) paraformaldehyde in PBS for 2 h. The samples were incubated 15 min with Atto 565-conjugated phalloidin (dilution 1:40, Molecular Probes) which stains actin filaments. Samples were then washed with PBS and the cell nuclei were stained with IM40-6 diamino-20-phenylindole in PBS (DAPI) (Molecular Probes). Fluorescence microscopy was performed with an Evos FL Cell Imaging System equipped with tree Led Lights Cubes (IEX (nm); IEM (nm)): DAPY (357/44; 447/60), GFP (470/22; 525/50), RFP (531/40; 593/40) from AMG (Advance Microscopy Group). Red channel was used to evaluate the cytoskeleton and blue for cell nucleus. All the experiments were carried out in triplicate.

2.5.2. Pre-osteoblast proliferation studies

The proliferation was determined by means of the Alamarblue[®] method at 1, 4, and 7 days of culture in contact with the different samples. The Alamarblue[®] method is based on the reduction of blue fluorogen (resazurin) to a red fluorescent compound (resofurin) by intracellular redox enzymes. A solution of resazurin sodium salt (Sigma Aldrich) at 0.01 mg/mL was prepared in phosphate-buffered saline (PBS) and then diluted 1:10 with culture medium supplemented with 10% FBS. The cells were exposed to resazurin solution for 3 h at 37°C under CO_2 (5%) atmosphere. Then fluorescence signal was read at $\lambda_{\text{em}} = 590 \text{ nm}$ using a $\lambda_{\text{exc}} = 560 \text{ nm}$ with a fluorescence spectrometer Biotek Synergy 4 device. Thereafter, the medium was renewed to continue the cell proliferation measurements at different times. Polystyrene culture plate was used as control and all the experiments were carried out in $n = 4$.

2.5.3. Pre-Osteoblasts early differentiation studies

The alkaline phosphatase (ALP) activity after 7 days in the presence of 1 mg/mL of the MBGs, was measured to evaluate the influence of the Ga as a differentiation marker in assessing the expression of the osteoblast phenotype. For this purpose, $3 \cdot 10^4$ MC3T3-E1 cells were seeded with a 1 mg/mL using supplemented medium with β -glycerol phosphate ($50 \text{ mg} \cdot \text{mL}^{-1}$, Sigma Chemical Company, St. Louis, MO, USA) and L-ascorbic acid (10 mM, Sigma Chemical Company, St. Louis, MO, USA). Solids were irrigated with PBS two times to remove as much residual serum possible. The cells were detached by subjecting the plates to cycles of freezing and thawing before measuring the ALP activity and total protein content. ALP activity was measured based on the hydrolysis of p-nitrophenylphosphate to p-nitrophenol. After 30 min incubation at 37°C the reaction was stopped by the addition of 125 μL of 2 M NaOH. The solution obtained was measured using a Helios Zeta UV-VIS spectrophotometer at 410 nm. Total protein content was determined using a colorimetric method at 540 nm (Bio-Analítica,S.L.) with a Helios Zeta UV-VIS spectrophotometer. Polystyrene culture plate was used as control and all the experiments were carried out in triplicate.

2.6. Osteoclasts culture tests

The mouse monocyte cell line RAW 264.7 was obtained from ATCC (Ref. # TIB-71; LGC Standards, Molsheim, France). Cells were

cultured in Dulbecco's Modified Eagle's Medium (DMEM, Gibco, Paisley, UK) containing 5% Hyclone serum (Thermo Scientific Braunschweig, Germany) and 1% penicillin/streptomycin (Gibco, Paisley, UK). For osteoclast differentiation experiments, RAW 264.7 cells were seeded at 5000 cells/cm² in alpha Minimum Essential Medium (α -MEM, Gibco, Paisley, UK) containing 5% Hyclone serum and effectors were added immediately. RANKL (Receptor Activator of Nuclear Factor- κ B Ligand) was used at 20 nM. Mouse effector GST-RANKL was produced as described by Strazić et al. [47], and a GST protein was produced and purified using the same protocol and was used as a control. Cells were cultured for four days with a renewal of the medium at day 2.

2.6.1. Viability assay

Raw 264.7 cells were seeded at a density of 5000 cells/cm² and treated with the different MBGs at 10 mg/mL or culture medium as control. After 4 days of incubation, the cells were incubated in a solution of 3-(4,5-dimethylthiazol-2-yl)-2,5-diphenyltetrazolium bromide (MTT) at 0.5 mg/mL for 4 h. Then, the MTT solution was removed and replaced by the same amount of the eluting buffer (DMSO/Ethanol 50:50). After 2 h agitation on an orbital shaker, 80 μ L of the colourful supernatant were transferred into a new 96-well plate which was read at 562 nm.

2.6.2. Tartrate-resistant acid phosphatase (ACP5) staining

Raw 264.7 cells were seeded as previously described and treated with the different types of MBGs (10 mg/mL) for 4 days. For control, cells were cultured without MBG. After 4 days, cells were rinsed two times in PBS and fixed in citrate/acetone solution for 30 s. ACP5⁺ cells were revealed using the Acid Phosphatase, Leukocyte kit following manufacturer's instructions (# 387A; Sigma-Aldrich, USA). Stained cells were observed using a light microscope (Axioplan 2, Zeiss, Germany) and the number of TRAP-positive multinucleated cells was evaluated by comparing 8 fields between the different treatments. To further quantify the TRAP staining, DMSO was added, and the plate was centrifuged for 15 min at 150 rpm at room temperature in dark. Finally, optical density at 562 nm was read [47].

2.7. Statistical analysis

The statistics data are expressed as means-standard deviations of experiments. Statistical analysis was performed using the Statistical Package for the Social Sciences (SPSS) version 11.5 software. Statistical comparisons were made by analysis of variance (ANOVA). Subsequently, post hoc analyses were carried out to correct for multiple comparisons. In all the statistical evaluations, $P < 0.05$ was considered as statistically significant.

3. Results

3.1. Physicochemical characterization of MBGs

The mesoporous structure of the MBGs was studied by XRD and TEM (Fig. 1). Both studies showed a disordered mesoporous structure for MBG-58S and MBG-58SGa materials, as usually found for MBGs with high calcium content. On the contrary, MBG-85S and MBG-85SGa exhibit a highly ordered hexagonal structure with planar group $p6mm$ and parallel channels with a d-spacing of 5–6 nm, similarly to the silica mesoporous material SBA-15 [48]. To obtain a deeper knowledge of the mesoporous structure, textural properties were analyzed by N₂ adsorption/desorption method. All the curves could be identified as type IV isotherms characteristic of mesoporous materials (Fig S1 in Supporting Information). Surface areas, pore volumes and pore sizes of the four MBGs are collected in

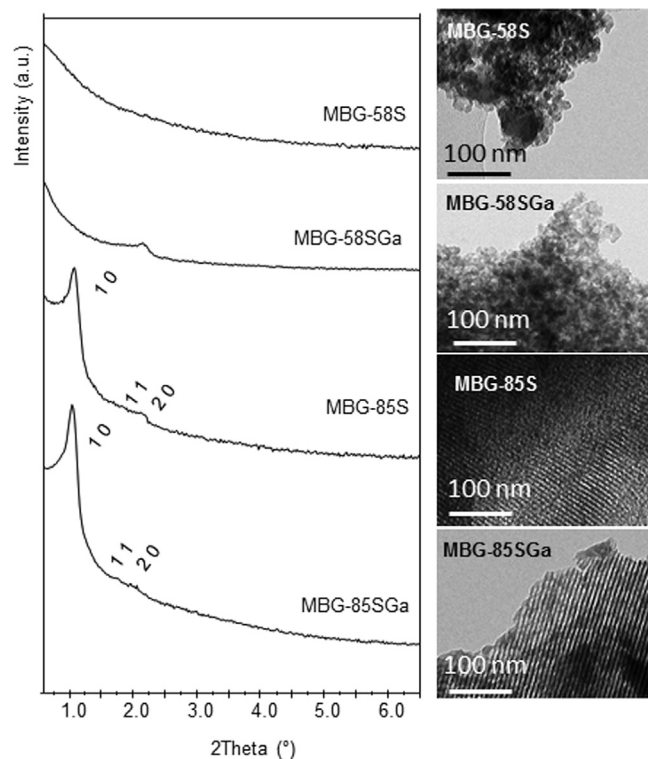


Fig. 1. Low angle XRD patterns (left) and TEM images of the different MBGs synthesized (right).

Table 2

Textural parameters obtained by N₂ adsorption porosimetry for the MBGs synthesized. Standard deviations are indicated in brackets.

Sample	Surface area (m ² ·g ⁻¹)	Pore volume (cm ³ ·g ⁻¹)	Pore size (nm)
MBG-58S	158.2 (±13.1)	0.14 (±0.05)	5.8 (±0.9)
MBG-58SGa	104.9 (±0.6)	0.23 (±0.01)	9.8 (±0.6)
MBG-85S	287.5 (±1.1)	0.29 (±0.04)	5.4 (±0.6)
MBG-85SGa	87.0 (±0.1)	0.12 (±0.07)	5.5 (±0.7)

Table 2. Gallium-free MBGs show surface areas and pore volumes of in the range commonly observed for MBGs when prepared with F127 as structure directing agent [8]. After Ga incorporation, a decrease of surface area and pore volume is observed for both compositions (MBG-58SGa and MBG-85SGa). Regarding pore size, Ga incorporation comprises a significant increment of this parameter for MBG-58SGa. On the contrary, pore size remains almost constant for MBG-85S after Ga incorporation.

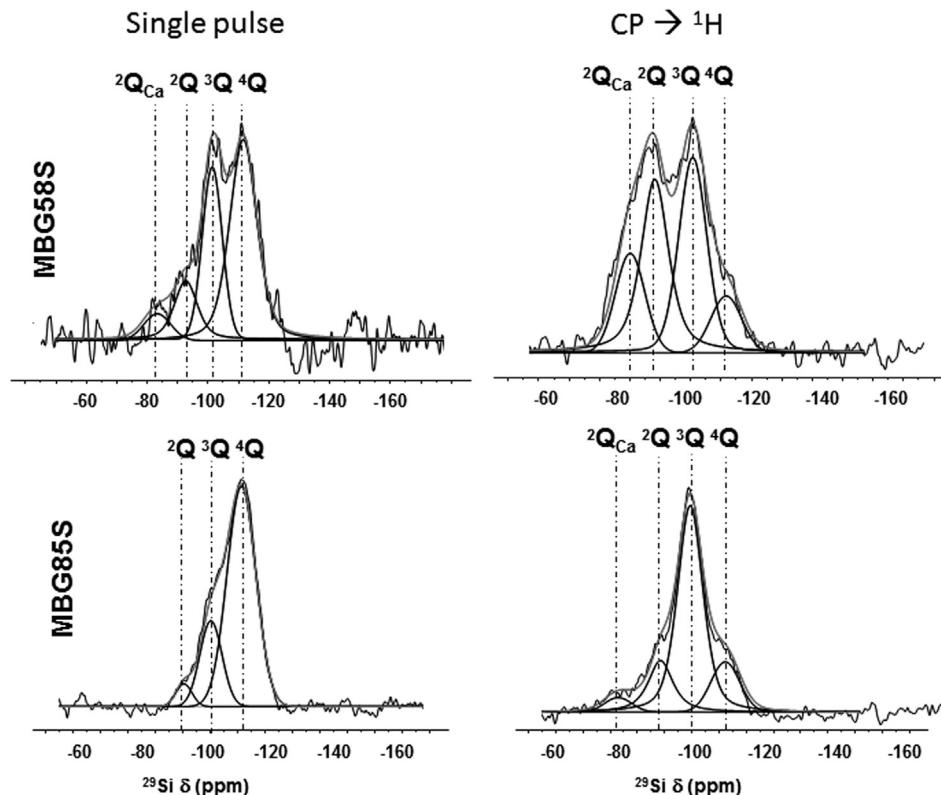
The chemical compositions of the MBGs are shown in Table 3. The incorporation of Ga³⁺ was carried out based on an ionic exchange with Ca²⁺ and the theoretical values displayed in Table 3 correspond to this assumption. The results obtained by XRF elemental analysis demonstrate that Ga incorporates to the MBGs in a very efficient way. In the case of MBG-58SGa, Ga incorporation is associated with a calcium loosening respect to MBG-58S, in agreement with the assumed mechanism that involved a Ca²⁺ versus Ga³⁺ ionic exchange. On the other hand, Ga incorporation within MBG-85SGa did not result in a significant calcium decrease.

To study the local atomic environment in the MBGs and the effect of Ga incorporation, solid-State ²⁹Si MAS NMR experiments were performed. Ga free MBGs (Fig. 2) show the resonances corresponding to the silicon species Q⁴, Q³, Q² and Q²_{ca} (with non-bonding oxygens associated to calcium cations). ¹H → ²⁹Si CP MAS spectra provide valuable information about the Si environment at

Table 3

Theoretical and experimental chemical compositions determined by XRF spectroscopy for the MBGs studied. Error values are indicated in brackets.

Sample	Theoretical composition (% mol) ^a	Experimental composition (% mol) ^b
MBG-58S	58 SiO ₂ – 37 CaO – 5 P ₂ O ₅	55.5 (0.20) SiO ₂ – 36.6 (0.15) CaO – 7.9 (0.11) P ₂ O ₅
MBG-58SGa	58 SiO ₂ – 31 CaO – 5 P ₂ O ₅ – 6 Ga ₂ O ₃	55.8 (0.25) SiO ₂ – 29.5 (0.18) CaO – 7.7 (0.1) P ₂ O ₅ – 7.0 (0.085) Ga ₂ O ₃
MBG-85S	85 SiO ₂ – 10 CaO – 5 P ₂ O ₅	85.2 (0.45) SiO ₂ – 10.6 (0.13) CaO – 4.2 (0.085) P ₂ O ₅
MBG-85SGa	85 SiO ₂ – 8.4CaO – 5P ₂ O ₅ – 1.6 Ga ₂ O ₃	83.5 (0.62) SiO ₂ – 10.2 (0.081) CaO – 4.3 (0.002) P ₂ O ₅ – 2.0 (0.05) Ga ₂ O ₃

^a Assuming that Ca²⁺ is substituted by Ga³⁺.^b Chemical composition determined by EDX spectroscopy.**Fig. 2.** Solid-state ²⁹Si single-pulse (left) and cross-polarization (right) MAS NMR spectra of Ga free MBGs.

the MBGs surface. The ¹H → ²⁹Si CP spectrum for MBG-58S decreases the intensity of the Q⁴ resonances and emphasizes the resonances for Q³ and Q² due to the presence of Si-OH groups at the MBG surface. The Q² resonance associated to the presence of Ca²⁺ is emphasized in a higher degree, pointing out that the MBG surface is enriched in Ca²⁺ with respect to the inner part of the MBG walls. On the other hand, MBG-85S does not show Q²(Ca²⁺) resonance in the single-pulse MAS spectrum and only a weak resonance can be observed in the ¹H → ²⁹Si CP experiment. After Ga incorporation, both single pulse and ¹H → ²⁹Si CP MAS spectra showed very similar results (Fig S2 in Supporting Information). The network connectivity of the different MBGs was calculated from the de-convoluted peak areas of single pulse spectra and are shown in Table 4. The results show that MBGs with higher Ca contents (MBG-58S and MBG-58SGa) have lower network connectivity compared to MBG-85S and MBG-85SGa. Moreover, ²⁹Si MAS NMR experiments indicate that the connectivity of the silica network is not significantly affected after Ga incorporation.

To probe the Ga local environment in the Ga-containing MBGs, ⁷¹Ga solid-state MAS NMR experiments were performed at very high magnetic field (20.0 T). As shown in Fig. 3, the experimental ⁷¹Ga central transition (CT) MAS NMR spectra of the MBGs exhibit two resolved resonances with asymmetric line shapes characteris-

tic of a distribution of the quadrupolar interaction. To account for this distribution, the ⁷¹Ga MAS NMR line shapes were reconstructed according to the Gaussian Isotropic Model (GIM) in which the distribution of the electric field gradient is assumed to correspond to a statistical disorder [49,50]. For the two observed resonances, the mean ⁷¹Ga isotropic chemical shifts determined from fits of the experimental spectra are characteristic of respectively six-fold ($\delta_{\text{ISO}} = 47$ ppm) and four-fold ($\delta_{\text{ISO}} = 172$ ppm) coordinated Ga in silicate environments, thus ruling out interaction between Ga ions and calcium phosphate groups [51–53]. This is also supported by the ³¹P MAS NMR spectra of the MBGs which remain similar before and after the Ga³⁺/Ca²⁺ exchange process (see Supporting information). For the two MBG compositions investigated, the ⁷¹Ga MAS NMR spectra therefore reveal that the Ga³⁺ cations are mainly incorporated in the silicate network as GaO₄ units (about 67 and 73% for MBG-58S and MBG-85S respectively) and that only a weak amount of them forms GaO₆ units (about 33 and 27% for MBG-58S and MBG-85S respectively). This suggests that Ga incorporation into MBG is not only related to a Ga/Ca exchange process but also involves the formation of GaO₄ units via Ga-O-Si covalent bonds. It should also be noted that the observed incorporation of GaO₄ units in the silicate network requires charge balancing which can be ensured either by Ca²⁺ or H⁺ cations.

Table 4
Relative peak areas and network connectivity (NC) of silica in MBGs, obtained by Solid-State Single Pulse ^{29}Si MAS NMR. Errors values are included in brackets.

Sample	Q^4	Q^3	Q^2	$Q^2 (X^{n+})^a$	N.C
MBG-58S	52.8 (0.47)	28.9 (0.86)	13.3 (0.85)	6.0 (0.78)	3.35
MBG-58SGa	30.2 (0.34)	41.9 (0.28)	18.4 (0.32)	9.4 (0.22)	3.37
MBG-85S	73.5 (0.58)	22.1 (0.83)	4.4 (0.15)	–	3.69
MBG-85SGa	70.3 (0.25)	24.2 (0.19)	5.6 (0.04)	–	3.64

^a Associated to Ca^{2+} and/or Ga^{3+} cations.

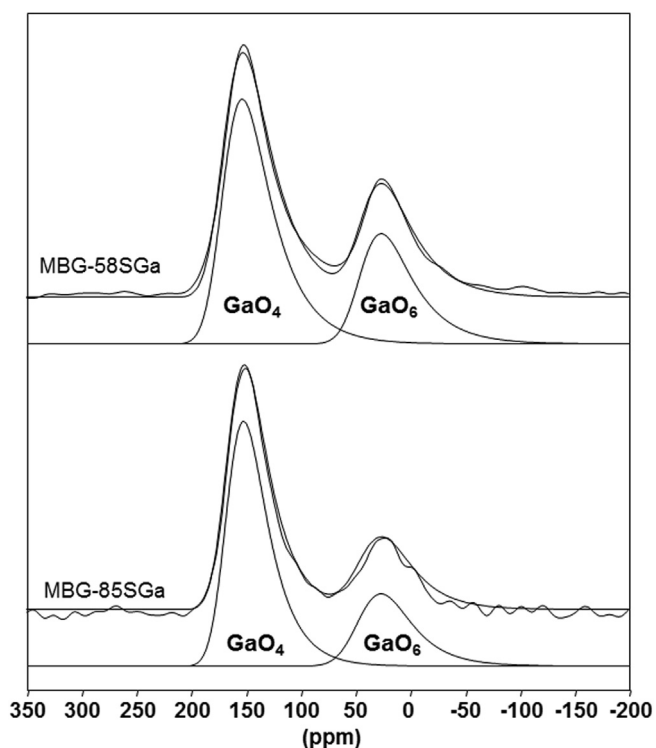


Fig. 3. ^{71}Ga solid state NMR MAS spectra of MBG-58SGa and MBG-85SGa and their deconvolution.

3.2. *In vitro* bioactivity test

Fig. 4 shows the Ca^{2+} concentration and pH values of SBF as a function of soaking time of the different MBGs. Calcium levels (**Fig. 4a**) increase for all the samples during the first 24 h and, the calcium concentration slowly decreases until the end of the assay. **Fig. 4b** plots the pH evolution of SBF as a function of soaking time, showing a decrease of H^+ concentration in SBF because of the ionic exchange with Ca^{2+} from the MBGs.

The evolution of the MBGs surfaces as a function of soaking time was followed by FTIR spectroscopy through. (**Fig S4 in Supporting Information**). Before soaking, the MBGs show a weak singlet absorption band at 600 cm^{-1} corresponding to the bending vibrational mode of phosphate groups in an amorphous environment, as correspond to P_2O_5 included in MBGs compositions. After 6 h in SBF, this band increases the intensity and split into a doublet at 560 and 610 cm^{-1} . The appearance of this doublet is commonly assigned to the formation of an apatite-like phase when bioactive glasses are in contact with SBF or similar biomimetic solutions [54]. In the case of MBG-58S and MBG-58SGa, an intense band at $1400\text{--}1550\text{ cm}^{-1}$ corresponding to the stretching vibrational mode of CO_3^{2-} groups increases as a function of soaking time, indicating

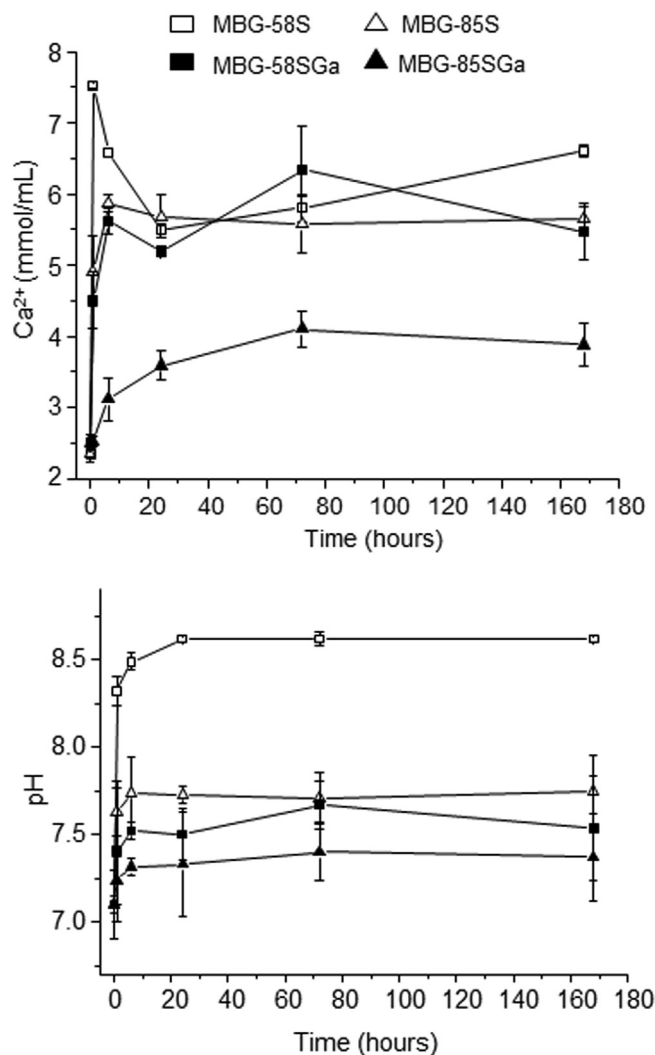


Fig. 4. Ionic dissolution in different media. (Top) Ca^{2+} concentration and (bottom) pH changes as a function of soaking time in SBF.

that the newly growth phase is a crystalline carbonated hydroxyapatite. This fact is related with the different morphology observed for the apatite crystallites in these samples. SEM observations at higher magnification (**Supporting information Fig. S6**) demonstrate that MBG-58S and MBG-58SGa develop an apatite phase made up of agglomerated spherical particles composed by very small crystallites, whereas MBG-85S and MBG85S-Ga form apatite with flake-shape morphology and larger crystallites.

Besides, the presence of a newly formed apatite like phase was confirmed by SEM (**Fig. 5**), indicating that, regardless the Ga presence or absence, the new apatite like phase nucleate and grows on these materials.

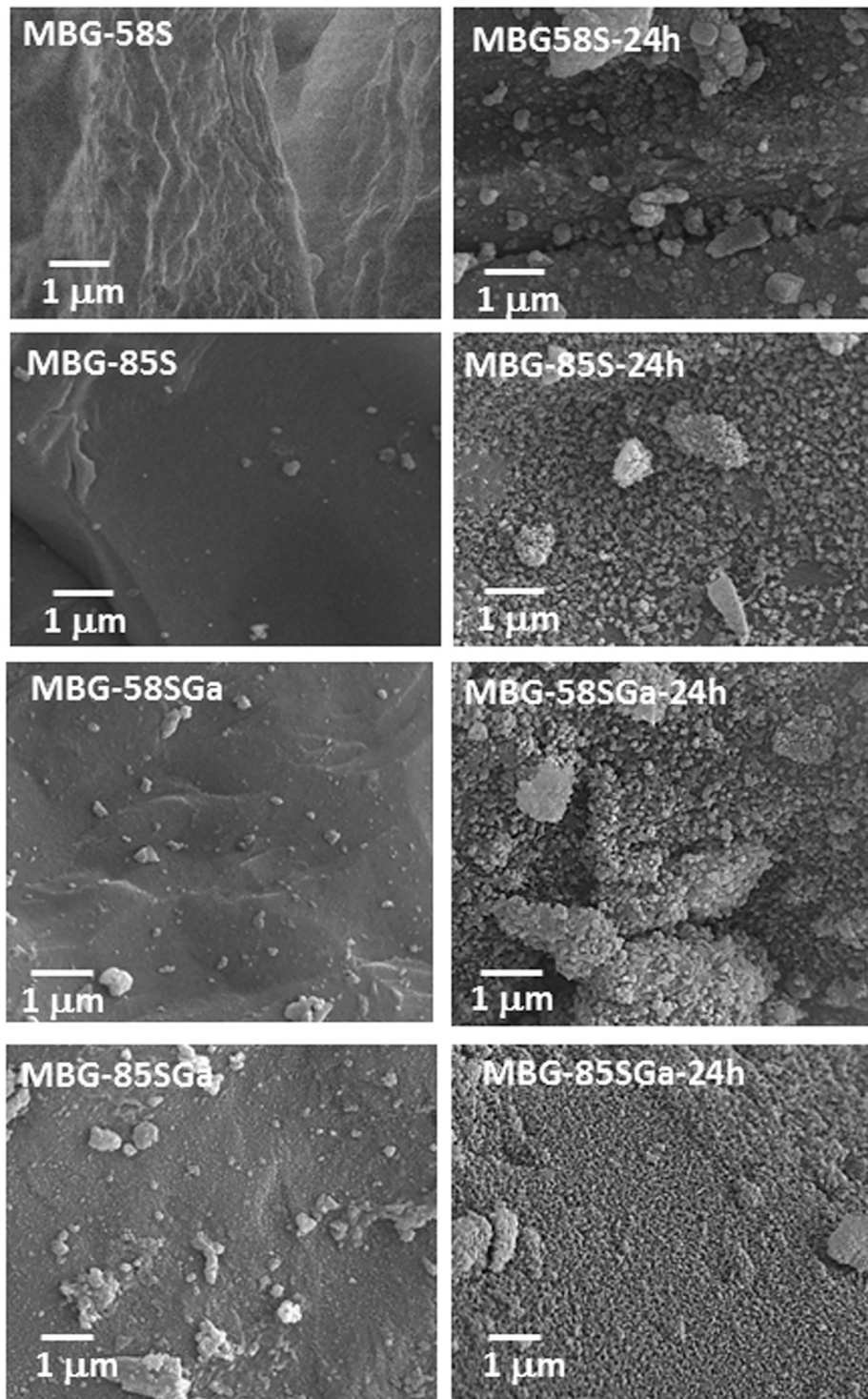


Fig. 5. SEM micrographs of the MBGs before (left) and after soaking in SBF for 24 h (right).

3.3. Ga *In vitro* release

Prior to put in contact the cells with the MBGs, we analysed the Ga solubility from the materials in α -MEM (Fig S7 in Supporting Information). After 7 days, Ga(III) concentration in α -MEM reached 803 μ M and 71 μ M for MBG-58SGa and MBG-85SGa, respectively. After 10 days, the concentrations of Ga released were 860 μ M and 86 μ M for MBG-58SGa and MBG-85SGa, respectively. These results indicate that, after this period, MBG-58SGa releases the 40% of the its gallium content whereas MBG-85SGa releases only the 12%.

3.4. Effect of Ga on MC3T3-E1 pre-osteoblast like cells

To evaluate Ga effect in osteoblastic bone forming cells, cell culture tests were carried out with MC3T3-E1 pre-osteoblast in the presence and absence of the materials for 1, 4 and 7 days. Fluorescence microscopy images (Fig. 6) show that MC3T3-E1 pre-osteoblast cultured in the presence of MBG are flattened and attached to the wells similarly to the cells in absence of materials (Supporting information Fig. S8). The cells show well-developed actin cytoskeletons organized into long parallel bundles, together

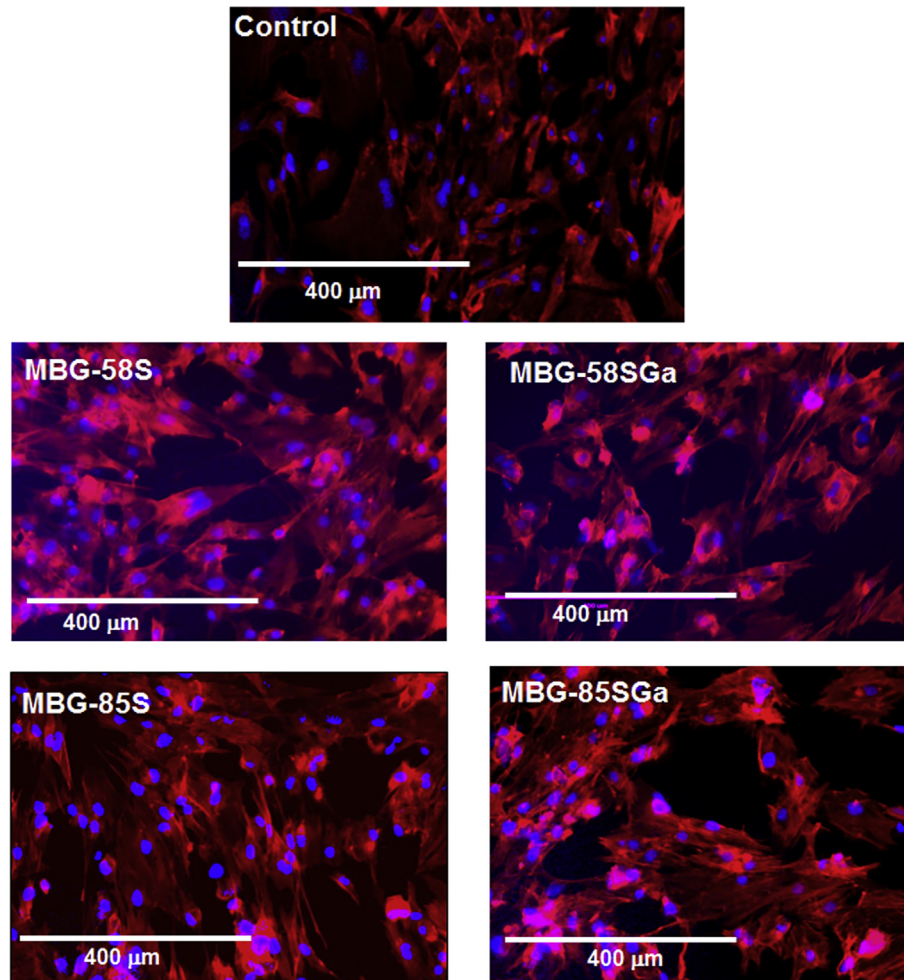


Fig. 6. Fluorescence microscopy images of MC3T3-E1 after 4 days in contact with MBGs. Some MBG particles are observed in purple. Control image shows MC3T3-E1 after 4 days in the absence of material. (For interpretation of the references to colour in this figure legend, the reader is referred to the web version of this article.)

with the nuclei in blue stained with DAPI. The purple bodies observed in the images correspond to MBGs particles that absorbed both stains in their mesoporous structure. MBG particles, which are in direct contact with MC3T3-E1 pre-osteoblast (Fig S9 in Supporting Information), do not lead to any morphological anomaly of the cytoskeleton.

Fig. 7a shows the proliferation of MC3T3-E1 in contact with MBGs. In agreement with the images observed by confocal microscopy, pre-osteoblast cells exhibit a good proliferative behaviour in contact with both, gallium free and gallium containing materials.

The effect of Ga on the MC3T3-E1 activity and early differentiation was studied by measuring the ALP and total protein after 7 days of incubation in contact with the materials (Fig. 7b). Significant differences in ALP activity were observed by comparing MBGs with and without Ga. In this case, MC3T3-E1 expressed higher ALP phosphatase activity when they were cultured in the presence of MBG-58SGa and MBG-85SGa, when compared to their Ga-free analogues.

3.5. Effect of Ga-doped MBGs on osteoclast cells

First, we measured the effect of the four different MBGs on the viability of RAW 264.7 monocytic cells stimulated with RANK-L (Fig. 8A). Compared to the control, both MBG-58S and MBG-85S significantly decreased the viability of RAW 264.7 (respectively 27 and 22%) but, Ga had no supplementary impact.

To evaluate the antiresorptive capability of Ga doped MBGs, the measurement of TRAP expression of mature osteoclasts has been carried out. The evaluation of positive multinucleated stained cells by microscopy let know that Ga dramatically affected the viability of mature OC whereas cells were normal when treated with control MBGs (i.e MBG-58S or MBG-85S). This inhibition is more pronounced in the case of MBG-85SGa. To quantify Ga effect on the osteoclast differentiation, we measured TRAP staining. We have previously demonstrated that TRAP quantification can be considered as a reliable marker of osteoclastogenesis [47]. Indeed, a correlation between the TRAP content per well and the number of TRAP + multinucleated cells per well has been observed. Fig. 8B evidences that the presence of Ga in MBG-58SGa and MBG-85SGa, strongly inhibited the expression of TRAP as compared to control condition.

4. Discussion

In this work we propose the incorporation of Ga(III) ions within MBGs as a strategy to improve the bone forming capability of these bioceramics. On the assumption that Ga(III) can inhibit osteoclastogenesis while fostering osteoblasts early differentiation, we envision that Ga-containing MBGs would be excellent bone grafting materials for osteoporotic patients. To understand the potential activity of Ga(III) ions over pre-osteoblasts and osteoclasts, we have carried out a deep physicochemical study, paying special

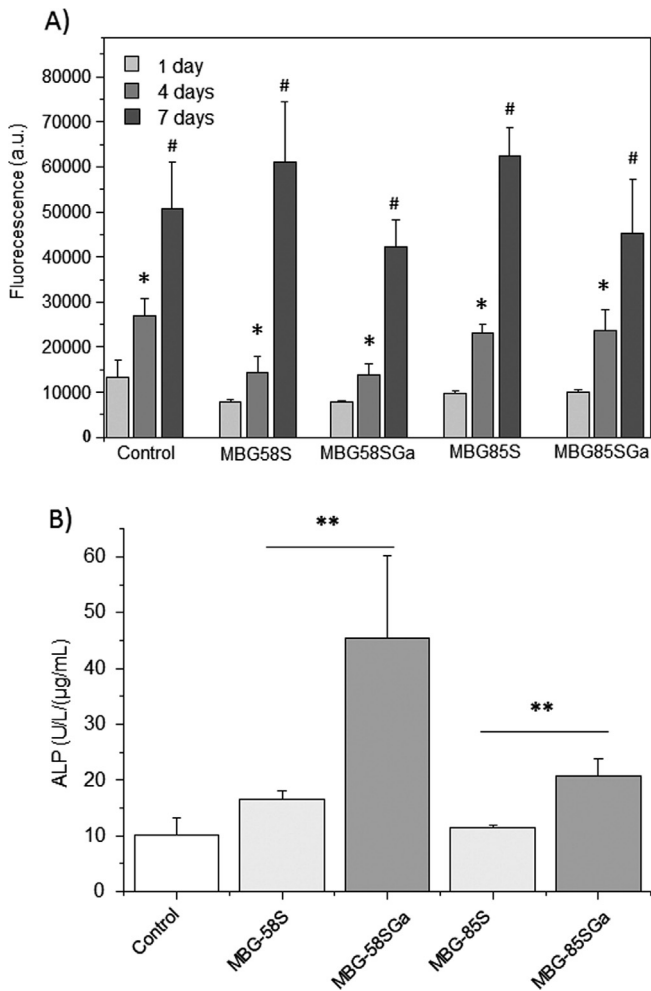


Fig. 7. (A) Proliferation of MC3T3-E1 pre-osteoblast like cells at 1, 4 and 7 days of culture in contact with the different MBGs synthesized. Statistical significance: * $p < 0.05$ (4 days vs 1 day) # $p < 0.01$ (7 days vs 4 days). (B) ALP activity of MC3T3-E1 pre-osteoblast like cells after 7 days of culture in contact with the different MBGs synthesized. Statistical significance: ** $p < 0.05$.

attention to the Ga local environment in Ga-containing MBGs. Our results demonstrate that Ga(III) ions are mainly incorporated as tetrahedral GaO_4 units. In this sense Ga(III) would covalently contribute as non-soluble species to the network connectivity of the $\text{SiO}_2\text{-CaO-P}_2\text{O}_5$ MBGs. The covalent bonding would be a consequence of the polycondensation of $[\text{GaO}_4]$ units with the $[\text{SiO}_4]$ tetrahedrons at the surface of MBGs, favoured by the alkaline conditions during the Ga incorporation process. This mechanism takes place in both MBG-58SGa and MBG-85SGa. Additionally, Ga(III) ions are also incorporated as $[\text{GaO}_6]$ octahedral species, thus acting as network modifiers and would constitute the main fraction of soluble Ga in MBGs. The incorporation of GaO_6 species occurs by means of Ca(II)-Ga(III) ionic exchange with Ca(II) cations of the MBGs. This second incorporation mechanism takes place to a higher extent in MBG-58SGa, as this composition contains more soluble Ca(II) ions acting as network modifiers in MBG-58S. During the Ca(II)-Ga(III) exchange, Ca^{2+} cations are released and the partial dissolution of MBG-58S takes place. Consequently, an enlargement of the pore size occurs, which is reflected in the higher values of pore size distribution observed for MBG-58SGa. In the case of MBG-85SGa, Ca(II)-Ga(III) exchange occurs to a lesser extent due to the smaller amount of Ca(II) available as network modifier. It must be highlighted that the presence of P_2O_5 as orthophosphate entraps most of the Ca^{2+} cations in calcium phosphate clusters,

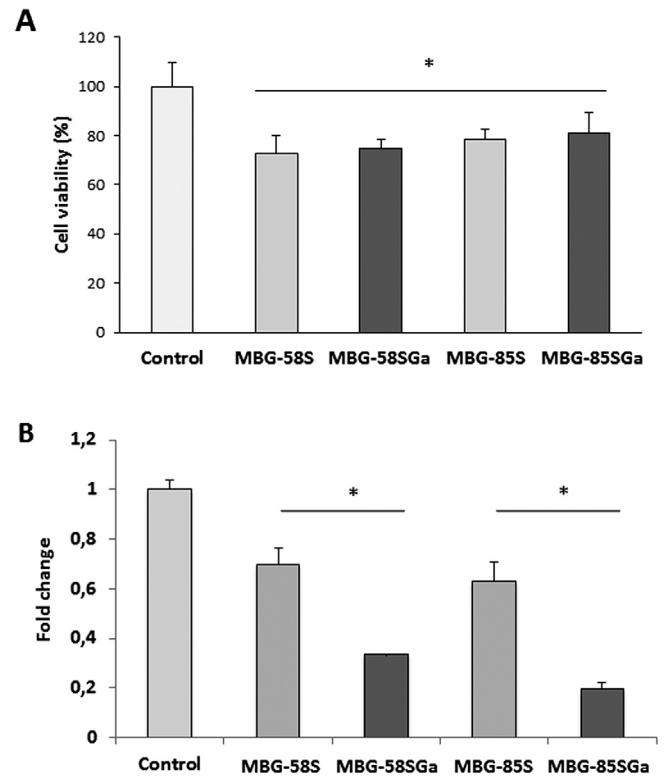


Fig. 8. (A) Viability of Raw 2647 mouse monocyte cells after 4 days of culture with 20 nM RANKL and in contact with 10 mg/ml of the different MBGs. (B) Effect of MBGs on the TRAP expression of mature OC. Cells were cultured for 4 days in presence of 20 nM RANKL. Then TRAP dosage of cellular extracts was performed, and optical density was read at 562 nm. Results were normalized according to control condition. * $p < 0.05$, statistically significant compared to control condition.

as could be observe by ^{31}P NMR studies and previously reported by our group [26–29]. In addition, the higher silica network connectivity of MBG-85S avoids the dissolution of this MBG during Ga(III) incorporation and, consequently, the pore size remains almost constant (Table 2). Depending on the composition of the MBG, surface area and porosity change differently after gallium incorporation. In the case of MBG-58SGa, it proceeds by means of calcium-gallium exchange. This mechanism involves the partial dissolution of MBG-58S, thus decreasing the surface area and increasing the pore size. On the other hand, MBG-85SGa evidences a higher decrease of surface area while keeping the pore size after gallium incorporation. These data point out that gallium mainly incorporates on the outer surface of MBG-85S without affecting the inner porous structure by dissolution. These results would agree with those obtained by Ga-NMR that indicate that gallium is mainly incorporate on MBG-85SGa through the polycondensation of $[\text{GaO}_4]$ units on the surface.

Despite of the Ca(II) decrease associated to Ga(III) incorporation, Ga-containing MBGs exhibit an excellent *in vitro* bioactive behavior. Both MBG-58SGa and MBG-85SGa developed an apatite like-layer on their surface after 6 h in contact with SBF. This test, although not definitive, is indicative of the osseointegration capability of this kind of materials under *in vivo* conditions [46,55]. In this sense, the high surface area and porosity of MBGs would be responsible of the high bioactivity, regardless the calcium loss.

Ga(III) ions do not affect pre-osteoblast proliferation and stimulate the early differentiation toward osteoblast phenotype. The increment of ALP activity of pre-osteoblasts in contact with Ga-containing MBGs respect to Ga-free MBGs indicate that this ion provides signals to stimulate differentiation toward bone forming cells. It must be highlighted that a very small amount

of Ga(III) in MBG-85SGa is enough to produce a significant increase of this early differentiation marker respect to MBG-85S. On the other hand, Ga incorporation in MBGs influences TRAP expression suggesting that the presence of Ga disturbs the osteoclastogenesis. These *in vitro* results are in concordance with our previous data relative to the biological effects of Ga in solution and loaded in a calcium phosphate matrix [36,56,57]. Interestingly, the activity of Ga has been closely related with its capability for being released as soluble species. At physiological pH, most of the dissolved Ga is present as gallate, $\text{Ga}(\text{OH})_4^-$ although the pH variability in the different bone compartments can modify both, solubility and speciation of Ga. In the case of our MBGs, although Ga solubility is very low (specially for MBG85S-Ga) is enough to inhibit osteoclastogenesis. After ten days in α -MEM, the released gallium reached 70 and 810 μmolar concentrations for MBG85S-Ga and MBG58S-Ga, respectively. Blair et al demonstrated that gallium concentrations between 7 and 12 μmolar in vivo and around 100 μmolar *in vitro*, are enough to promote inhibition of osteoclastogenesis [58]. In this sense, both MBGs would be able to supply soluble gallium species to impact on the cultured cells. However, it must be highlighted that osteoclast inhibition is more pronounced in the case of MBG-85SGa, although the amount of Ga released is much lower compared to MBG-58SGa. This fact suggests that gallium bonded at the MBG85S-Ga surface is active, similarly to the experiment of Hall and Chambers, who demonstrated that bonded gallium to bone remain active [32]. In fact, in the case of MBG85S-Ga, gallium is mainly incorporated at the external surface of the MBG85S as indicated by the dramatic reduction of textural properties after Ga incorporation (Table 3). Our results suggest that, in addition to the solubilized gallium, this element would be also incorporated into macrophages in contact with MBG particles, thus inhibiting the differentiation toward osteoclast phenotype.

5. Conclusions

Mesoporous bioactive glasses in the system $\text{SiO}_2\text{-CaO-P}_2\text{O}_5\text{-Ga}_2\text{O}_3$ have been prepared by impregnation of Ga(III) on two different $\text{SiO}_2\text{-CaO-P}_2\text{O}_5$. Ga (III) incorporation proceeds according to two different mechanisms: direct condensation within the silica network and ionic exchange with Ca (II), resulting in the formation of network formers GaO_4 units and network modifiers GaO_6 .

The incorporation of Ga within $\text{SiO}_2\text{-CaO-P}_2\text{O}_5$ MBGs does not inhibit their excellent bioactive behavior.

The presence of Ga in MBGs shows a selective behavior with respect to different cell types. Whereas Ga-doped MBGs stimulate the early differentiation of pre-osteoblast towards osteoblastic phenotype, our experiments also demonstrate that Ga disturbs the osteoclastogenesis. Interestingly, these effects of Ga on bone cells does not require the dissolution of this element.

Considering the excellent bioactive behavior of $\text{SiO}_2\text{-CaO-P}_2\text{O}_5\text{-Ga}_2\text{O}_3$ based MBGs and their selective behavior with respect to osteoblasts and osteoclasts, these bioceramics might be considered as excellent bone substitutes for regenerative purposes in osteoporotic patients.

Acknowledgements

This study was supported by research grants from the Ministerio de Economía y Competitividad (projects MAT2015-64831-R and MAT2016-75611-R AEI/FEDER, UE. M.V.-R. acknowledges funding from the European Research Council (Advanced Grant VERDI; ERC-2015-AdG Proposal 694160).

Appendix A. Supplementary data

Supplementary data associated with this article can be found, in the online version, at <https://doi.org/10.1016/j.actbio.2018.06.036>.

References

- [1] X. Yan, C. Yu, X. Zhou, J. Tang, D. Zhao, Highly ordered mesoporous bioactive glasses with superior in vitro bone-forming bioactivities, *Angew. Chemie. Int. Ed.* 43 (2004) 5980–5984.
- [2] X. Yan, X. Huang, C. Yu, H. Deng, Y. Wang, Z. Zhang, S. Qiao, G. Lu, D. Zhao, The in-vitro bioactivity of mesoporous bioactive glasses, *Biomaterials* 27 (2006) 3396–3403.
- [3] A. López-Noriega, D. Arcos, I. Izquierdo-Barba, Y. Sakamoto, O. Terasaki, M. Vallet-Regí, Ordered mesoporous bioactive glasses for bone tissue regeneration, *Chem. Mater.* 18 (2006) 3137–3144.
- [4] X. Chen, Y. Zhao, S. Geng, R.J. Miron, Q. Zhang, C. Wu, Y. Zhang, In vivo experimental study on bone regeneration in critical bone defects using PIB nanogels/boron-containing mesoporous bioactive glass composite scaffold, *Int. J. Nanomed.* 10 (2015) 839–846.
- [5] N. Cheng, Y. Wang, Y. Zhang, B. Shi, The osteogenic potential of mesoporous bioglasses/silk and non-mesoporous bioglasses/silk scaffolds in ovariectomized rats: in vitro and in vivo evaluation, *PLoS ONE* 8 (2013) e81014.
- [6] C. Wu, J. Chang, Mesoporous bioactive glasses: structure characteristics, drug/growth factor delivery and bone regeneration application, *Interface Focus* 2 (2012) 292–306.
- [7] M. Vallet-regí, D. Arcos, Mesoporous materials for biomedical applications, in: P.J. Pannone (Ed.), *Trends in Biomaterials Research*, Nova Science Publishers Inc, 2007, pp. 109–142.
- [8] N. Gómez-Cerezo, I. Izquierdo-Barba, D. Arcos, M. Vallet-Regí, Tailoring the biological response of mesoporous bioactive materials, *J. Mater. Chem. B* (2015) 3810–3819.
- [9] J.R. Jones, Reprint of: review of bioactive glass: from hench to hybrids, *Acta Biomater.* 23 (2015) 53–82.
- [10] L.L. Hench, I.D. Xynos, J.M. Polak, Bioactive glasses for in situ tissue regeneration, *J. Biomater. Sci. Polym. Ed.* 15 (2004) 543–562.
- [11] I.D. Xynos, A.J. Edgar, L.D.K. Buttery, L.L. Hench, J.M. Polak, Gene-expression profiling of human osteoblasts following treatment with the ionic products of Bioglass®45S5 dissolution, *J. Biomed. Mater. Res.* 55 (2001) 151–157.
- [12] I.D. Xynos, M.V.J. Hukkanen, J.J. Batten, L.D. Buttery, L.L. Hench, J.M. Polak, Bioglass®45S5 stimulates osteoblast turnover and enhances bone formation in vitro: implications and applications for bone tissue engineering, *Calcif. Tissue Int.* 67 (2000) 321–329.
- [13] I. Izquierdo-Barba, D. Arcos, Y. Sakamoto, O. Terasaki, A. López-Noriega, M. Vallet-regí, High-performance mesoporous bioceramics mimicking bone mineralization, *Chem. Mater.* 20 (2008) 3191–3198.
- [14] C. Wu, J. Chang, Multifunctional mesoporous bioactive glasses for effective delivery of therapeutic ions and drug/growth factors, *J. Control. Release* 193 (2014) 282–295.
- [15] Y. Li, Y.Z. Liu, T. Long, X. Bin Yu, T.T. Tang, K.R. Dai, B. Tian, Y.P. Guo, Z.A. Zhu, Mesoporous bioactive glass as a drug delivery system: fabrication, bactericidal properties and biocompatibility, *J. Mater. Sci. Mater. Med.* 24 (2013) 1951–1961.
- [16] M. Zhu, J. Shi, Q. He, L. Zhang, F. Chen, Y. Chen, An emulsification-solvent evaporation route to mesoporous bioactive glass microspheres for bisphosphonate drug delivery, *J. Mater. Sci.* 47 (2012) 2256–2263.
- [17] F. Wang, D. Zhai, C. Wu, J. Chang, Multifunctional mesoporous bioactive glass/upconversion nanoparticle nanocomposites with strong red emission to monitor drug delivery and stimulate osteogenic differentiation of stem cells, *Nano Res.* 9 (2016) 1193–1208.
- [18] L. Polo, N. Gómez-Cerezo, E. Aznar, J. Vivancos, F. Sancenón, D. Arcos, M. Vallet-Regí, R. Martínez-Mañez, Molecular gates in mesoporous bioactive glasses for the treatment of bone tumors and infection, *Acta Biomater.* 50 (2017) 114–126.
- [19] H.M. Lin, W.K. Wang, P.A. Hsiung, S.G. Shyu, Light-sensitive intelligent drug delivery systems of coumarin-modified mesoporous bioactive glass, *Acta Biomater.* 6 (2010) 3256–3263.
- [20] P. Han, C. Wu, J. Chang, Y. Xiao, The cementogenic differentiation of periodontal ligament cells via the activation of Wnt/a-catenin signalling pathway by Li^+ ions released from bioactive scaffolds, *Biomaterials* 33 (2012) 6370–6379.
- [21] Y. Zhang, L. Wei, J. Chang, R.J. Miron, B. Shi, S. Yi, C. Wu, Strontium-incorporated mesoporous bioactive glass scaffolds stimulating in vitro proliferation and differentiation of bone marrow stromal cells and in vivo regeneration of osteoporotic bone defects, *J. Mater. Chem. B* 1 (2013) 5711.
- [22] J. Ye, J. He, C. Wang, K. Yao, Z. Gou, Copper-containing mesoporous bioactive glass coatings on orbital implants for improving drug delivery capacity and antibacterial activity, *Biotechnol. Lett.* 36 (2014) 961–968.
- [23] C. Wu, Y. Zhou, W. Fan, P. Han, J. Chang, J. Yuen, M. Zhang, Y. Xiao, Hypoxia-mimicking mesoporous bioactive glass scaffolds with controllable cobalt ion release for bone tissue engineering, *Biomaterials* 33 (2012) 2076–2085.

- [24] C. Wu, R. Miron, A. Sculean, S. Kaskel, T. Doert, R. Schulze, Y. Zhang, Proliferation, differentiation and gene expression of osteoblasts in boron-containing associated with dexamethasone deliver from mesoporous bioactive glass scaffolds, *Biomaterials* 32 (2011) 7068–7078.
- [25] R. Mathew, P.N. Gunawidjaja, I. Izquierdo-Barba, K. Jansson, A. García, D. Arcos, M. Vallet-regí, Ed, Solid-State ^{31}P and ^1H NMR Investigations of Amorphous and Crystalline Calcium Phosphates Grown Biomimetically From a Mesoporous Bioactive Glass, *J. Phys. Chem.* (2011) 0–10.
- [26] E. Leonova, I. Izquierdo-Barba, D. Arcos, A. López-Noriega, N. Hedin, M. Vallet-Regí, M. Edén, Multinuclear solid-State NMR studies of ordered mesoporous bioactive glasses, *J. Phys. Chem. C* 112 (2008) 5552–5562.
- [27] P.N. Gunawidjaja, R. Mathew, A.Y.H. Lo, I. Izquierdo-Barba, A. García, D. Arcos, M. Vallet-Regí, M. Edén, Local structures of mesoporous bioactive glasses and their surface alterations in vitro: inferences from solid-state nuclear magnetic resonance, *Philos. Trans. R. Soc. A* 370 (2012) 1376–1399.
- [28] R. Mathew, C. Turdean-Ionescu, B. Stevansson, I. Izquierdo-Barba, A. García, D. Arcos, M. Vallet-Regí, M. Edén, Direct probing of the phosphate-ion distribution in bioactive silicate glasses by solid-state NMR: evidence for transitions between random/clustered scenarios, *Chem. Mater.* 25 (2013) 1877–1885.
- [29] A. García, M. Cicuéndez, I. Izquierdo-Barba, D. Arcos, M. Vallet-Regí, Essential role of calcium phosphate heterogeneities in 2D-hexagonal and 3D-cubic $\text{SiO}_2\text{-CaO-P}_2\text{O}_5$ mesoporous bioactive glasses, *Chem. Mater.* 21 (2009) 5474–5484.
- [30] A. Philippart, N. Gómez-Cerezo, D. Arcos, A.J. Salinas, E. Boccacchi, M. Vallet-Regí, A.R. Boccacchi, Novel ion-doped mesoporous glasses for bone tissue engineering: study of their structural characteristics influenced by the presence of phosphorous oxide, *J. Non. Cryst. Solids* 455 (2017) 90–97.
- [31] P. Ridefelt, E. Gylfe, G. Akerström, J. Rastad, Effects of the antihypercalcemic drugs Ga nitrate and pamidronate on hormone release of pathologic human parathyroid cells, *Surgery* 117 (1995) 56–61.
- [32] T.J. Hall, T.J. Chambers, Ga inhibits bone resorption by a direct effect on osteoclasts, *Bone Miner.* 8 (1990) 211–216.
- [33] R.S. Bockman, A.L. Boskey, N.C. Blumenthal, N.W. Alcock, R.P. Warrell, Ga increases bone calcium and crystallite perfection of hydroxyapatite, *Calcif. Tissue Int.* 39 (1986) 376–381.
- [34] M.A. Repo, R.S. Bockman, F. Betts, A.L. Boskey, N.W. Alcock, R.P. Warrell Jr., Effect of Ga on bone mineral properties, *Calcif. Tissue Int.* 43 (1988) 300–306.
- [35] R.P. Warrell, Ga nitrate for the treatment of bone metastases, *Cancer* 80 (1997) 1680–1685.
- [36] E. Verron, M. Masson, S. Khoshniat, L. Duplomb, Y. Wittrant, M. Baud'Huin, Z. Badran, B. Bujoli, P. Janvier, J.C. Scimeca, J.M. Boulter, J. Guicheux, Ga modulates osteoclastic bone resorption in vitro without affecting osteoblasts, *Br. J. Pharmacol.* 159 (2010) 1681–1692.
- [37] E. Verron, J.M. Boulter, J.C. Scimeca, Ga as a potential candidate for treatment of osteoporosis, *Drug Discov Today* 17 (2012) 1127–1132.
- [38] C. Mellier, F. Fayon, F. Boukhechba, E. Verron, M. Leferrec, G. Montavon, J. Lesoeur, V. Schnitzler, D. Massiot, P. Janvier, O. Gauthier, J. Boulter, B. Bujoli, Design and properties of novel Ga-doped injectable apatitic cements, *Acta Biomater.* 24 (2015) 322–332.
- [39] S. Shruti, F. Andreatta, E. Furlani, E. Marin, S. Maschio, L. Fedrizzi, Cerium, Ga and zinc containing mesoporous bioactive glass coating deposited on titanium alloy, *Appl. Surf. Sci.* 378 (2016) 216–223.
- [40] S. Shruti, A.J. Salinas, G. Lusvardi, G. Malavasi, L. Menabue, M. Vallet-Regí, Mesoporous bioactive scaffolds prepared with cerium- Ga- and zinc-containing glasses, *Acta Biomater.* 9 (2013) 4836–4844.
- [41] S. Shruti, A.J. Salinas, E. Ferrari, G. Malavasi, G. Lusvardi, A.L. Doadrio, L. Menabue, M. Vallet-Regí, Curcumin release from cerium, Ga and zinc containing mesoporous bioactive glasses, *Microporous Mesoporous Mater.* 180 (2013) 92–101.
- [42] A.J. Salinas, S. Shruti, G. Malavasi, L. Menabue, M. Vallet-Regí, Substitutions of cerium, Ga and zinc in ordered mesoporous bioactive glasses, *Acta Biomater.* 7 (2011) 3452–3458.
- [43] S. Pourshahrestani, E. Zeimaran, N. Adib Kadri, N. Gargiulo, S. Samuel, S.V. Naveen, T. Kamarul, M.R. Towler, Ga-containing mesoporous bioactive glass with potent hemostatic activity and antibacterial efficacy, *J. Mater. Chem. B* 4 (2016) 71–86.
- [44] C.J. Brinker, Y. Lu, A. Sellinger, H. Fan, Evaporation-induced self-assembly: nanostructures made easy, *Adv. Mater.* 11 (1999) 579–585.
- [45] B.M. Fung, A.K. Khitrin, K. Ermolaev, An improved broadband decoupling sequence for liquid crystals and solids, *J. Magn. Reson.* 142 (2000) 97–101.
- [46] T. Kokubo, H. Kushitani, S. Sakka, T. Kitsugi, T. Yamamuro, Solutions able to reproduce in vivo surface-structure changes in bioactive glass-ceramic, *J. Biomed. Mater. Res.* 24 (1990) 721–734.
- [47] I. Strazic-Geljic, I. Guberovic, B. Didak, H. Schmid-Antomarchi, A. Schmid-Alliana, F. Boukhechba, J.-M. Boulter, J.-C. Scimeca, E. Verron, Ga, a promising candidate to disrupt the vicious cycle driving osteolytic metastases, *Biochem. Pharmacol.* 116 (2016) 11–21.
- [48] D. Zhao, Q. Huo, J. Feng, B.F. Chmelka, G.D. Stucky, Nonionic triblock and star diblock copolymer and oligomeric surfactant syntheses of highly ordered, hydrothermally stable, mesoporous silica structures, *J. Am. Chem. Soc.* 120 (1998) 6024–6036.
- [49] B. Bureau, G. Silly, J. Buzaré, C. Legein, D. Massiot, From crystalline to glassy Ga fluoride materials: an NMR study of ^{69}Ga and ^{71}Ga quadrupolar nuclei, *Solid State Nucl. Magn. Reson.* 14 (1999) 181–190.
- [50] G. Czjzek, J. Fink, F. Götz, H. Schmidt, J.M.D. Coey, J.-P. Rebouillat, A. Liénard, Atomic coordination and the distribution of electric field gradients in amorphous solids, *Phys. Rev. B* 23 (1981) 2513–2530.
- [51] C.-F. Cheng, H. He, W. Zhou, J. Klinowski, J.A.S. Gonçalves, L.F. Gladden, Synthesis and characterization of the gallosilicate mesoporous molecular sieve MCM-41, *J. Phys. Chem.* 100 (1996) 390–396.
- [52] V. Montouillout, C.M. Morais, A. Douy, F. Fayon, D. Massiot, Towards a better description of gallo-phosphate materials in solid state NMR: 1D and 2D correlation studies, *Magn. Reson. Chem.* 44 (2006) 770–775.
- [53] C. Mellier, F. Fayon, V. Schnitzler, P. Deniard, M. Allix, S. Quillard, D. Massiot, J.-M. Boulter, B. Bujoli, P. Janvier, Characterization and properties of novel Ga-doped calcium phosphate ceramics, *Inorg. Chem.* 50 (2011) 8252–8260.
- [54] A.L.B. Maçon, T.B. Kim, E.M. Valliant, K. Goetschius, R.K. Brow, D.E. Day, A. Hoppe, A.R. Boccacchi, I.Y. Kim, C. Ohtsuki, T. Kokubo, A. Osaka, M. Vallet-Regí, D. Arcos, L. Fraile, A.J. Salinas, A.V. Teixeira, Y. Vueva, R.M. Almeida, M. Miola, C. Vitale-Brovarone, E. Verné, W. Höland, J.R. Jones, A unified in vitro evaluation for apatite-forming ability of bioactive glasses and their variants, *J. Mater. Sci. Mater. Med.* 26 (2015) 115–124.
- [55] M. Bohner, J. Lemaitre, Can bioactivity be tested in vitro with SBF solution?, *Biomaterials* 30 (2009) 2175–2179.
- [56] I. Strazic-Geljic, N. Melis, F. Boukhechba, S. Schaub, C. Mellier, P. Janvier, J.-P. Laugier, J.-M. Boulter, E. Verron, J.-C. Scimeca, Ga enhances reconstructive properties of a calcium phosphate bone biomaterial, *J. Tissue Eng. Regen. Med.* 12 (2018) e854–e866.
- [57] E. Verron, A. Loubat, G.F. Carle, C. Vignes-Colombeix, I. Strazic, J. Guicheux, N. Rochet, J.M. Boulter, J.C. Scimeca, Molecular effects of Ga on osteoclastic differentiation of mouse and human monocytes, *Biochem. Pharmacol.* 83 (2012) 671–679.
- [58] H.C. Blair, S.L. Teitelbaum, H.L. Tan, P.H. Schlesinger, Reversible inhibition of osteoclastic activity by bone-bound gallium (III), *J. Cell Biochem.* 48 (1992) 401–410.